

# Space Weather®



## RESEARCH ARTICLE

10.1029/2025SW004427

### Key Points:

- We describe a newly collected long-period magnetotelluric (MT) data set covering Scotland, England and Wales
- We derive a geoelectric field model based on MT data from 70 sites to assess the impact of geomagnetic activity on grounded infrastructure
- Comparing geoelectric fields from three significant geomagnetic storms shows high amplitudes not only in Scotland but also in northern England

### Correspondence to:

J. Hübert,  
juliane.huebert@bgs.ac.uk

### Citation:

Hübert, J., Eaton, E., Beggan, C. D., Montiel-Álvarez, A. M., Kiyan, D., & Hogg, C. (2025). Developing a new ground electric field model for geomagnetically induced currents in Britain based on long-period magnetotelluric data. *Space Weather*, 23, e2025SW004427. <https://doi.org/10.1029/2025SW004427>




Received 10 MAR 2025

Accepted 18 JUL 2025

### Author Contributions:

**Conceptualization:** J. Hübert, E. Eaton, C. D. Beggan, A. M. Montiel-Álvarez  
**Data curation:** J. Hübert, E. Eaton, A. M. Montiel-Álvarez  
**Formal analysis:** J. Hübert  
**Methodology:** J. Hübert, E. Eaton, C. D. Beggan, A. M. Montiel-Álvarez  
**Project administration:** C. D. Beggan  
**Resources:** D. Kiyan, C. Hogg  
**Validation:** J. Hübert, C. D. Beggan  
**Visualization:** J. Hübert  
**Writing – original draft:** J. Hübert

## Developing a New Ground Electric Field Model for Geomagnetically Induced Currents in Britain Based on Long-Period Magnetotelluric Data

J. Hübert<sup>1</sup> , E. Eaton<sup>1,2</sup>, C. D. Beggan<sup>1</sup> , A. M. Montiel-Álvarez<sup>3</sup> , D. Kiyan<sup>4</sup>, and C. Hogg<sup>4</sup>

<sup>1</sup>British Geological Survey, Edinburgh, UK, <sup>2</sup>University of Leeds, Leeds, UK, <sup>3</sup>University of Edinburgh, Edinburgh, UK, <sup>4</sup>Dublin Institute for Advanced Studies, Dublin, Ireland

**Abstract** Large variations in ground electric field in mid-latitude countries like the UK during a geomagnetic storm drive so-called geomagnetically induced current, a major geohazard to ground-based technological infrastructure like electrical transformers at high voltage substations, gas pipelines and railway signaling. In order to assess these effects, the ground electric field response over a large bandwidth of signal periods from seconds to hours needs to be known. In the UK, this was previously done using a thin sheet model of electrical conductivity based on airborne electromagnetic and laboratory measurements. More accurately, the geoelectric fields can be modeled from magnetotelluric (MT) measurements. Here we describe the recent collection of MT data at 53 sites across Britain. The recorded timeseries data of geomagnetic and geoelectric fields were processed into MT impedance tensors at each site. We complemented the data set with MT legacy data to a total of 70 sites. Using the spherical elementary current system approach to interpolate ground magnetic field variations in the UK at each site, we convolve these with the MT impedance tensors to compute the modeled geoelectric field across Britain for three major geomagnetic storms of the past decades: March 1989, October 2003, and September 2017. During the larger geomagnetic storms of 1989 and 2003 we observe that the modeled amplitude of geoelectric fields is not solely determined by latitude but also locally by the geology. The largest electric fields are surprisingly found in central Britain, reaching 12 V/km during the March 1989 storm.

**Plain Language Summary** Geomagnetic storms driven by space weather create time-varying magnetic fields in the ionosphere which penetrate into the ground creating induced electric fields. These geoelectric fields are usually harmless and dissipate locally. However, grounded man-made technology can allow them to equalize over longer distances through infrastructure like the high voltage power grid. To accurately predict the geoelectric field during geomagnetic storms requires so-called magnetotelluric (MT) measurements. These consist of short-term (4–6 weeks) recordings of simultaneous magnetic and electric field data at the same site to understand how a magnetic field change locally creates an electric field response due to the geology. We collected data at 53 sites between 2021 and 2024 to make a new map for the island of Great Britain. We investigate the predicted geoelectric fields using magnetic measurements from three of the largest geomagnetic storms in the past 35 years.

## 1. Introduction

During severe space weather events, the Earth's magnetic field can interact and couple with the solar wind and undergo large variations in the order of thousands of nT at mid-latitudes within short time frames (Rogers et al., 2020; Thomson et al., 2011). These temporal variations of the externally-driven magnetic field induce an electric field in the Earth, whose magnitude and spatial scale depend on the underlying electrical conductivity structure of the rocks at crustal and mantle depths.

Strong geoelectric fields, which can rise to several tens of V/km in some locations (Love et al., 2018), build up over large areas and pose a hazard to certain types of modern technology. The architecture of low-resistance grounded infrastructure, such as high voltage (HV) power networks and gas pipelines, allows these induced geoelectric fields to equalize through their earthing points, typically in substations. These quasi-steady DC currents are called Geomagnetically Induced Currents (GICs) and, though small in comparison to the electric current carried, are a threat to the safe and optimal operation of HV transformers (Boteler, 2006; Pulkkinen et al., 2012). A well-known example of extreme damage from GICs is the failure of the Québec-Hydro network in

© 2025 British Geological Survey © UKRI.

This is an open access article under the terms of the [Creative Commons Attribution License](#), which permits use, distribution and reproduction in any medium, provided the original work is properly cited.

March 1989 (Bolduc, 2002; Boteler, 2019). The present-day cost of a similar widespread and long-lasting power outage could be of the order of tens of billions of US dollars per day (Oughton et al., 2018).

GICs are therefore recognized as a potential hazard to electrical power transmission systems across the world, particularly at higher latitudes or in regions with lengthy high-voltage transmission lines. The first step in understanding this hazard is to quantify the induced geoelectric field at the Earth's surface. Unfortunately, long-term measurements of the geoelectric field are rare and only performed at a few locations around the world including Hungary, Japan, the USA and the UK. Most hazard assessment relies on numerical geoelectric field modeling. While there are different approaches to model geoelectric fields during geomagnetic storm times, all need to take the electrical conductivity of the Earth into account. The electrical conductivity of the earth down to large depths (e.g., >250 km beneath cratons) can be derived from magnetotelluric (MT) measurements.

Depending on the availability of data and models, research on space weather impacts from geoelectric fields have been derived using 1D conductivity distributions (Turnbull, 2010), 2D models (Beggan et al., 2013), 2.5D (Rosenqvist & Hall, 2019) and full 3D models (Kruglyakov et al., 2022; Marshalko et al., 2021). When large-scale MT data are available, using a direct data approach of convolving MT impedances with time-series of magnetic fields has become popular (Campanya et al., 2019; Cordell et al., 2021; Kelbert et al., 2017; Malone-Leigh et al., 2023; Pratscher et al., 2024). In Britain, the MT data approach was used by Hübert et al. (2024) in a validation study for measured and modeled GICs.

Magnetotelluric surveying is a widely used electromagnetic (EM) deep-sounding method to image the subsurface electrical conductivity (or its inverse, the electrical resistivity) in varying scales, from shallow subsurface to crustal targets and global induction studies. MT has been used extensively in mineral exploration, geothermal and environmental surveys and to investigate tectonic and volcanic settings, but data sets are often commercially valuable and therefore hard to access for further research (Ayala et al., 2022). The depth of investigation depends on the period or frequency of the recorded signal variations in the magnetic and electric field at the surface of the Earth. Longer period/lower frequency signals penetrate deeper into the crust, whereas higher frequencies (short periods) probe the shallower subsurface. Long-period MT (LMT) employs fluxgate magnetometers to capture the magnetic field variations and is mostly utilized to study the structure of the lower crust and mantle. For shallower targets, higher frequency data are collected with broadband equipment including induction coil magnetometers.

In the past few decades, an added value of existing MT data over larger regional scales was recognized because it can be used to help characterize space weather impacts on ground infrastructure through modeling of the ground electric field during geomagnetically active times. Where few MT data exist, there is a need to collect new and to reuse older legacy data sets. In the UK, due to the absence of large MT data sets, the initial attempts to characterize the ground electrical conductivity involved synthetic models based on geologic data and lithological considerations. A thin-sheet conductance model of the upper 3 km was developed for space weather use (Beamish, 2013; McKay, 2003), based on airborne electromagnetic (EM) data and laboratory measurements of electrical conductivity of bedrock samples, superimposed on 1D regions of lithospheric conductivity based on defined geologic terranes. With this model, regional electrical fields were computed using the thin-sheet approach first conceived by Vasseur and Weidelt (1977), albeit with relatively large uncertainties (Beggan, 2015).

To address the scarcity of MT data in the UK, in 2021 a new campaign to measure MT at up to 50 sites with a better than 70 km spatial resolution was embarked upon. In this study, we describe the methodology, data collection and processing and present the new data. We then estimate the likely magnitude of the geoelectric field generated during past large geomagnetic storms, assessing the dependence of local geology on the geoelectric hazard.

## 2. A New Geoelectric Field Model for Britain

Time-varying electric and magnetic fields occur naturally in the ground, driven by external field variations; they induce each other as expressed through Maxwell's equations. The ground electric, or geoelectric, field during geomagnetic storms is induced by the disturbed geomagnetic field. The geoelectric field exhibits much larger lateral variation than the magnetic field because electrical charge carriers are very unevenly distributed in the subsurface. The ability to transport electric current in rocks is captured in the bulk electrical conductivity (resistivity) and the amplitude and direction of the geoelectric field is directly dependent on the conductivity distribution in the subsurface. Electrical conductivity is a wide-ranging rock parameter and depends mostly on the composition, pore space and fluid content of the rocks (Karato & Wang, 2013). For example, a porous fluid-

saturated sandstone is a much better conductor than a dense young granite. The best electrical conductors in the context of geology are metals, melts, fluids and graphite. Ground electric fields are generally quite small (in the range of mV/km) and can be measured via the potential difference between two metallic electrodes. For longer term measurements, non-polarizable electrodes are needed to avoid the build-up of charges due to electrochemical reactions.

To capture the electric field over an area as large as the British Isles in real-time, we would need to deploy a large number of instruments (at least 50) to continuously measure the geoelectric field. However, permanent deployment of this instrumentation is expensive and would require a huge amount of resources to quality-check, repair and maintain such a network. In the UK, the ground electric field is currently monitored at three sites (the BGS geomagnetic observatories in Lerwick, Eskdalemuir and Hartland) and the data collected there were described in Beggan et al. (2021). The sparse number of direct observation sites of the electric field make it necessary to develop numerical models to cover the gaps between measurement locations and allow for modeling of space weather impacts.

## 2.1. The Magnetotelluric Method

The MT method is a deep-sounding geophysical technique that uses the principles of EM induction to study the interior of the Earth (Cagniard, 1953). By simultaneously recording the variations in the natural magnetic and electric field on the surface of the Earth it is possible to infer models of underlying electrical conductivity (Chave & Jones, 2012). In practice, a magnetic sensor samples the magnetic field in Cartesian coordinates (x-north, y-east, z-downwards) every second. For long period recordings this is a three-axial fluxgate magnetometer. The horizontal electric field is measured along two perpendicular dipoles. The recorded time-series are filtered and transformed into frequency spectra which can then be used to derive the impedance tensor  $Z$ . The impedance tensor is defined in the frequency domain ( $\omega = 2\pi/f$ ) and as a transfer function of the variation of the magnetic field ( $B$ ) to that of the electric field ( $E$ ):

$$E(\omega) = Z(\omega) \cdot B(\omega)$$

The  $Z$  tensor has four complex components:

$$Z = \begin{pmatrix} Z_{xx} & Z_{xy} \\ Z_{yx} & Z_{yy} \end{pmatrix}$$

and is often displayed as apparent resistivity (a measure for the amplitude and the true resistivity if the subsurface is homogeneous) and phase curves for each component. These allow for a quick visual inspection of the magnitude and changes in conductivity in the subsurface with depth.

The inducing magnetic field is assumed to be spatially uniform, and  $Z$  is considered quasi-stationary (i.e., independent of when the recordings were performed) and only dependent on the local Earth response (geology). In the absence of active geologic processes (e.g., volcanic) that change the composition or electrical conductivity of the underlying rocks,  $Z$  is assumed to be stable in time. Typically, recording at an MT location lasts from a few days to a couple of months. The length and quality of the data determines the frequency range of the computed transfer function, with the depth of investigation controlled by the skin-depth of the EM waves. Assuming a plane wave magnetic field impulse is driving the induced geoelectric field, the derived impedance tensor can be used to estimate the induced geoelectric field in a wide frequency range at any time when only magnetic field data are available (Campanya et al., 2019; Hübert et al., 2020; Malone-Leigh et al., 2023). Thus, the MT impedance tensor only needs to be correctly measured once and can be used to compute an estimate of any future (or past) geoelectric field if a magnetic field time series at the location is available.

## 2.2. New Long-Period Magnetotelluric Data in Britain

Within the UK-funded Space Weather Innovation Measurement Modeling and Risk (SWIMMR) Activities in Ground Effects (SAGE) project (Beggan et al., 2025), a campaign to collect new MT data across England and Wales was initiated. The aim was to complement existing MT data and to make measurements across Great Britain with approximately evenly-distributed 50–70 km distance between sites, omitting large urban centers;

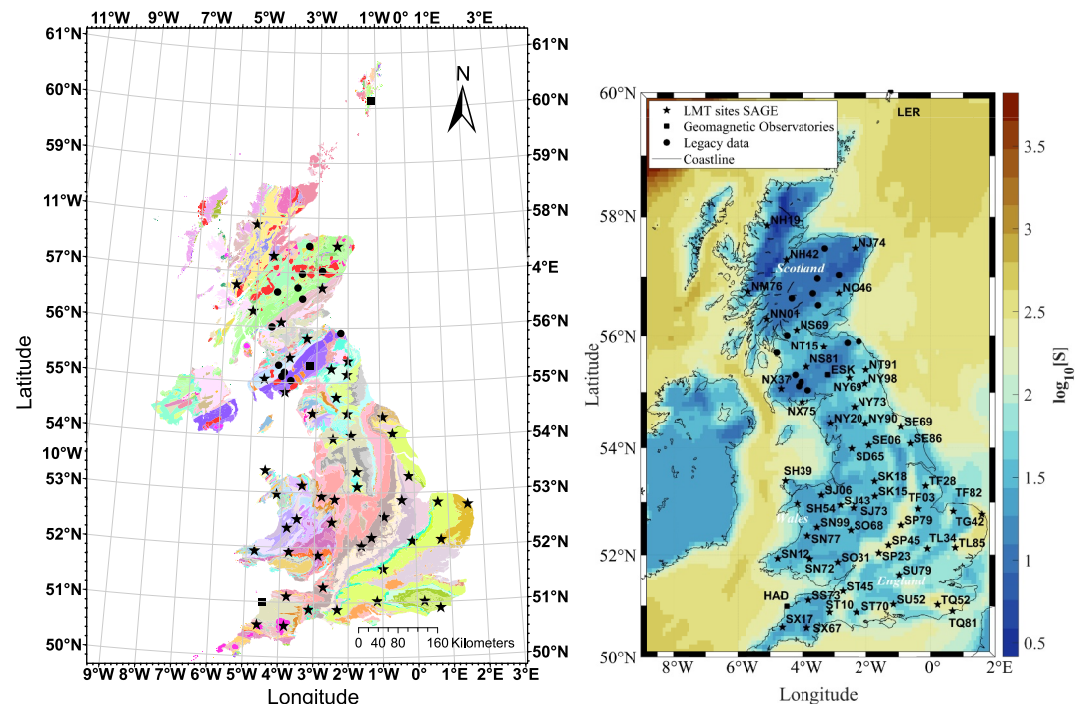


**Figure 1.** Left: Location of SWIMMR Activities in Ground Effects (SAGE) magnetotelluric (MT) sites (see also Table 1) and bedrock geology map of the UK. Squares—BGS geomagnetic observatories, stars—new long-period MT (LMT) sites collected 2021–2024, circles—legacy MT sites. For the geologic units see the BGS geology index viewer. <https://www.bgs.ac.uk/map-viewers/bgs-geology-viewer/>. Contains OS data Crown Copyright and database right 2020. Right: Conductance map of the British Isles, based on the bedrock conductivity map from Beamish (2012) and location of MT sites with site names using a reference to the UK grid reference.

similar to other large-scale field campaigns (Dong et al., 2013; Duan, 2019; Schultz, 2009). Since MT is a passive method where signal-noise ratios are site-dependent, careful selection of site locations is a priority. Ideally, sites are well away from all man-made EM signal sources like electrified railway lines (>10 km), electric fences and power lines (>1 km), industry (>5 km), housing and generators (>2 km), similar to the recommendation for magnetic observations (Jankowski & Sucksdorff, 1996). Data collection for long-period signals takes at least three to 4 weeks, so the site should be in an rural area mostly undisturbed by people or livestock. At each chosen site, all sensors were buried to about half a meter depth and well away from tree roots. All cables were buried in shallow trenches to avoid damage from weather or animals. As far as possible, we pre-selected sites using satellite imagery and open-source information available with respect to the location of railway and power lines.

For the SAGE field campaign, three Lemi-417 and one Lemi-424 MT instrument including fluxgate magnetometers and Cu/CuSo<sub>4</sub> electrodes were used. Due to the travel restrictions during the Covid-19 pandemic, the intended start of the field campaign was delayed from October 2020 to April 2021, with data collection continuing until March 2024. MT site installations followed a rolling approach with continuous deployment of the four MT systems in use (see Figure 2). We installed on average two to three sites each month. In total, 44 new LMT sites were installed in England and Wales between April 2021 and August 2023 (Hübner et al., 2025). Nine additional sites were collected in Scotland during October 2023 to March 2024 (Montiel-Álvarez et al., 2025). We chose a naming convention based on the British Ordnance Survey grid references, with two letters and two numbers. This gives an approximate location to 10 km resolution and more importantly allows us to incorporate older sites and legacy measurements with a location-keyed naming convention. The locations of MT sites collected can be seen in Figure 1 with a bedrock geology map of the UK. Geomagnetic activity was relatively quiet during the field campaign (see lower panel in Figure 2 for the aa index), but several smaller geomagnetic storms were recorded (see Figure 3). Increased geomagnetic activity usually also improves the quality of MT transfer function estimates.

Time-series processing to derive MT impedance tensors was performed using the processing code of Smirnov (2003). Remote referencing (e.g., Egbert, 1997; Gamble et al., 1979) was applied using UK observatory data



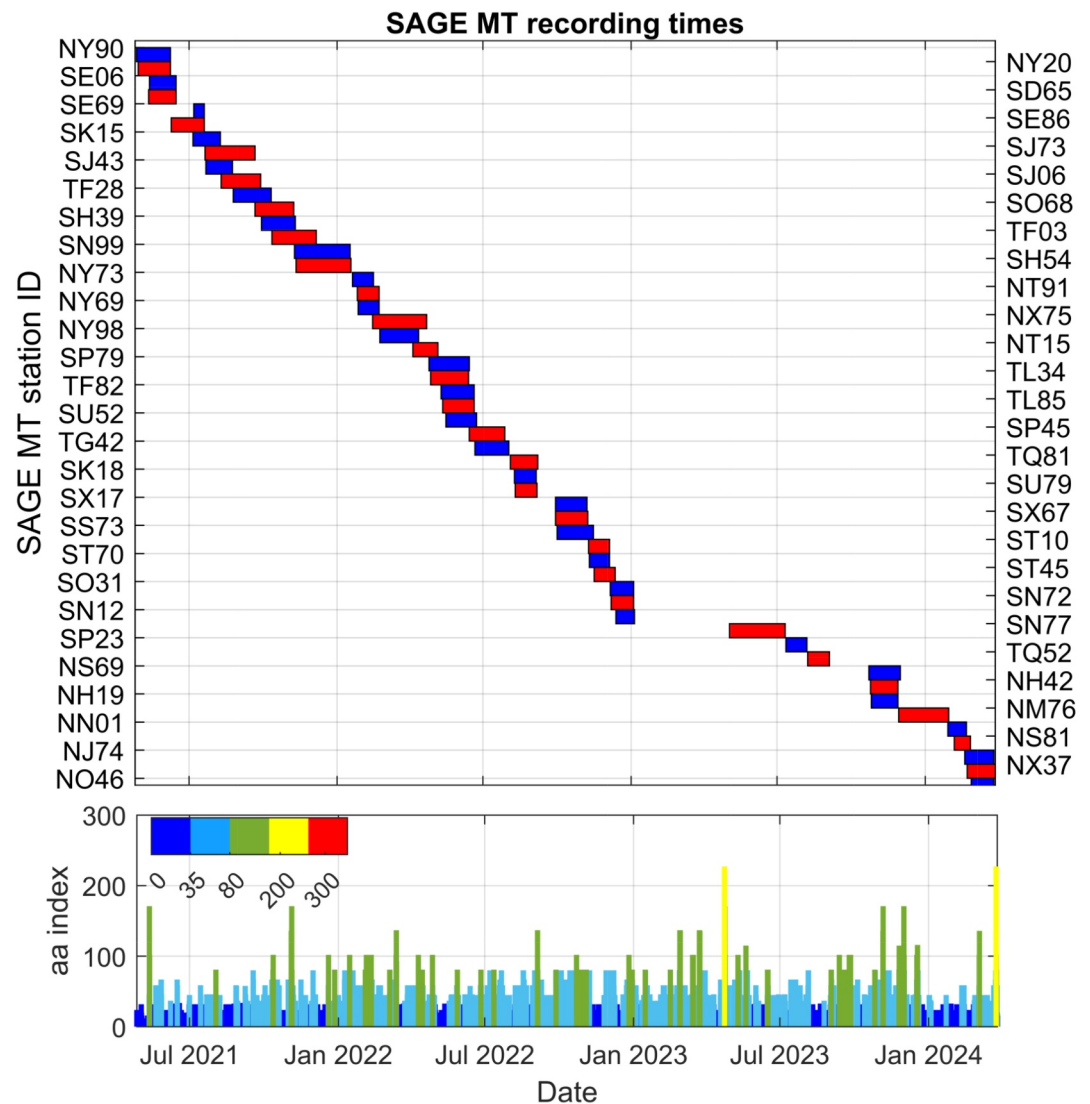


**Figure 2.** Upper panel: Deployment schedule of SAGE long-period MT sites. Lower panel: The *aa* geomagnetic activity index in units of *nT*. The *aa* index is a simple indicator for global geomagnetic activity, derived from the *K* index of two geomagnetic observatories, currently Hartland in the UK and Canberra in Australia.

(mostly from Eskdalemuir, ESK) and simultaneous recordings to improve the impedance data quality by reducing local noise. The frequency-dependent impedances for three sites are presented in Figure 4 as apparent resistivity and phase of the impedance tensor elements. The magnitude of the apparent resistivity gives an indication of the variability of electrical conductivity across Britain and will also influence the amplitude of geoelectric fields during storms, with higher apparent resistivities facilitating larger ground currents.

### 2.3. Legacy Magnetotelluric Data in Britain

Magnetotelluric data in the UK have been collected for several decades, but only a few data sets have been archived in data repositories while some are only preserved as paper copies. To complement the new MT data, the following existing data sets were used to extend the coverage:

- MT impedances were calculated at the three UK observatories (Lerwick LER, Hartland HAD, Eskdalemuir ESK) using long-term magnetic and electric field recordings (Beggan et al., 2021).

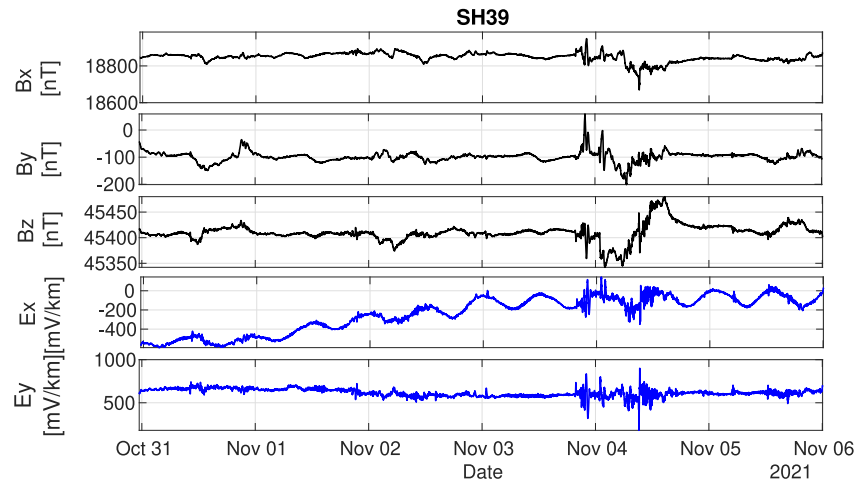


**Figure 3.** Example of a raw magnetotelluric time-series recorded during six days in 2021 during the SAGE field campaign: Three magnetic field components ( $B_x$ ,  $B_y$ ,  $B_z$ ) and the two horizontal electric field components ( $E_x$ ,  $E_y$ ) at site SH39 in Wales. A short G3 storm occurred on 4 November 2021. Note a strong tidal signal is visible in  $E_x$ , superimposed on a longer term instrumental drift.

- Simpson and Bahr (2021): Seven LMT stations were collected in Scotland (2017–2019) as part of a larger data set within a previous space weather project. The available time-series data are sampled at 32 s which limits the frequency bandwidth and not all data from this survey had sufficiently high data quality. Data were retrieved from the UK National Geoscience Data Center (NGDC) hosted by the BGS.

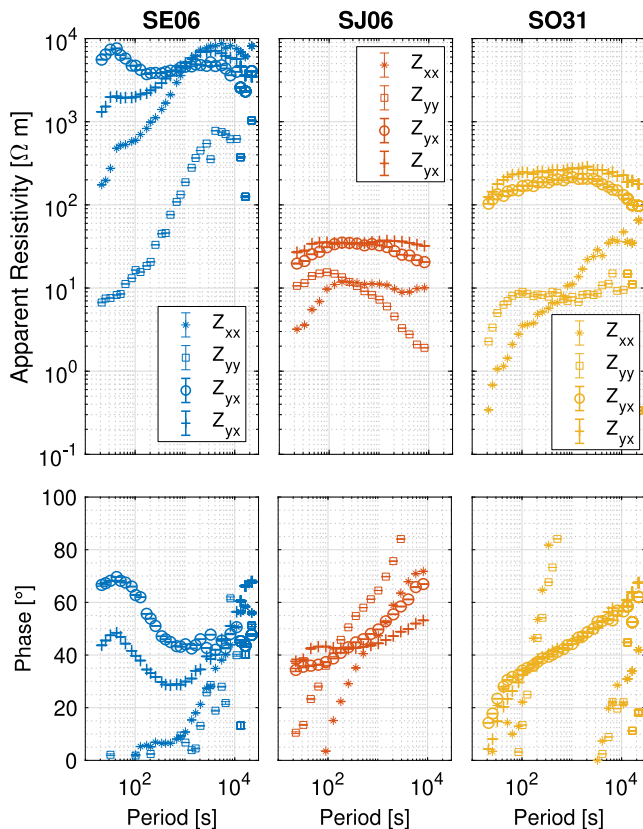


**Figure 4.** Example for magnetotelluric impedance tensors estimated at three SWIMMR Activities in Ground Effects sites (SE06, SJ06 and SO31, for their location see Figure 1). Data are displayed as apparent resistivity (upper panels) and phase (lower panels) for all four components of the impedance tensor for periods of 16–20,000 s.

- Hübert et al. (2020): Two LMT stations collected in east and west Scotland in 2018, with full frequency bandwidth available. These data are also accessible at the NGDC.
- Banks (pers comm): A collection of legacy MT data in Scotland recorded before 1999 by the University of Edinburgh were kindly made available by Roger Banks (Junge, 1995; Livelybrooks et al., 1993). The original time-series data are not available, only the processed impedance tensors with limited frequency bandwidth. We selected the best quality sites from visual inspection.
- Tauber et al. (2003): A broadband survey was carried out in Dumfries and Galloway (Scotland). This was part of a larger data set which has previously been used for space weather impact studies (e.g., McKay, 2003). The original time-series raw data are not available, only the authors' estimates of the impedance tensor. Four of the visually best sites were chosen with the widest possible geographical spread of site locations within this array.

In total, data from 70 MT sites (Table 1) are used in the following modeling section. These provide the foundation for the first purely data-driven geoelectric field model in Britain to assess space weather ground impacts. In a final step to prepare the data for geoelectric field modeling, we harmonized the impedance tensors from the SAGE and legacy data sets before the geoelectric field modeling by excluding periods longer than 20,000 s, smoothing the transfer functions with a moving average and a factor of 1.5 and interpolating onto seven values per frequency decade.

For the geoelectric field modeling in this study, the MT impedances for periods between 120 s and 20,000 s are used, due to the cadence of 1 min of the available geomagnetic data. While it is envisaged that geomagnetic real-time data will be available with a 1 s sampling rate in the near future, the standard

**Table 1**  
*Location of Magnetotelluric Sites Used in This Study*

#	Grid ref/name	Location	Latitude [°]	Longitude[°]	Collected by
1	NY90	Richmond	54.44067	−2.02602	BGS
2	NY20	Lake District	54.44425	−3.11343	BGS
3	SE06	Appletreewick	54.04938	−1.91066	BGS
4	SD65	Forest of Bowland	53.98667	−2.4656	BGS
5	SE69	North Yorkshire	54.38460	−0.92516	BGS
6	SE86	Scarborough	54.07972	−0.62928	BGS
7	SK15	Derbyshire	53.11447	−1.72591	BGS
8	SJ73	Market Drayton	52.88483	−2.40687	BGS
9	SJ43	Wrexham	52.93861	−2.80353	BGS
10	SJ06	Denbigh	53.13584	−3.39858	BGS
11	TF28	Lincoln	53.305	−0.15539	BGS
12	SO68	Shropshire Hills	52.46889	−2.49063	BGS
13	SH39	Anglesey	53.39774	−4.52626	BGS
14	TF03	Grantham	52.86825	−0.38476	BGS
15	SN99	Caersws	52.52497	−3.53213	BGS
16	SH54	Porthmadog	52.97288	−4.15874	BGS
17	NY73	Alston	54.74057	−2.37553	BGS
18	NT91	Alnham	55.40232	−2.00772	BGS
19	NY69	Kielder Forest	55.25962	−2.53405	BGS
20	NX75	Dumfries	54.83088	−3.99212	BGS
21	NY98	Kirkwhelpington	55.15623	−2.03917	BGS
22	NT15	Nine Mile Burn	55.81058	−3.32239	BGS
23	SP79	Market Harborough	52.56506	−0.92253	BGS
24	TL34	Cambridge	52.1239	−0.10123	BGS
25	TF82	Houghton Hall	52.82396	0.69672	BGS
26	TL85	Shimpling	52.14081	0.75420	BGS
27	SU52	Hinton Ampner	51.03599	−1.15631	BGS
28	SP45	Banbury	52.1887	−1.30625	BGS
29	TG42	Long Gores Marsh	52.76779	1.59098	BGS
30	TQ81	Pett Level	50.90340	0.67191	BGS
31	SK18	Landybower	53.38953	−1.73748	BGS
32	SU79	Christmas Common	51.61645	−0.97164	BGS
33	SX17	Bodmin Moor	50.58792	−4.62314	BGS
34	SX67	Dartmoor	50.57599	−3.85067	BGS
35	SS73	Exmoor	51.11418	−3.79573	BGS
36	ST10	Blackdown Hills	50.87845	−3.14719	BGS
37	ST70	Hazelbury Bryan	50.87684	−2.32016	BGS
38	ST45	Cheddar Gorge	51.28881	−2.73186	BGS
39	SO31	East Brecon Beacons	51.86291	−2.88986	BGS
40	SN72	West Brecon Beacons	51.92524	−3.75579	BGS
41	SN12	Pembrokeshire	51.93279	−4.76363	BGS
42	SN77	Aberystwyth	52.36339	−3.82800	BGS
43	SP23	Burmington	52.03775	−1.60521	BGS

**Table 1**  
*Continued*

#	Grid ref/name	Location	Latitude [°]	Longitude[°]	Collected by
44	TQ52	High Weald AONB	51.02692	0.21575	BGS
45	NS64	Kippen	56.09486	−4.17646	UoE+BGS
46	NH42	Drumnadrochit	57.30094	−4.49182	UoE+BGS
47	NH19	Leckmelm	57.86257	−5.09354	UoE+BGS
48	NM76	Acharacle	56.754192	−5.68861	UoE+BGS
49	NN01	Inveraray	56.28728	−5.10666	UoE+BGS
50	NS81	Abington	55.45744	−3.86357	UoE+BGS
51	NJ74	Turriff	57.49136	−2.35532	UoE+BGS
52	NX37	Newton Stewart	55.06196	−4.65605	UoE+BGS
53	NO46	Forfar	56.72884	−2.85449	UoE+BGS
Observatories:					
54	HU43	Lerwick observatory	60.13839	−1.18119	BGS
55	NT20	Eskdalemuir observatory	55.31677	−3.20702	BGS
56	SS22	Hartland observatory	50.99499	−4.48498	BGS
Legacy sites:					
57	NT66	Whiteadder	55.88319	−2.59097	BGS (SWIGS)
58	NS24	Dalry	55.70406	−4.78822	BGS (SWIGS)
59	NS48	CAL	56.00383	−4.47334	UoS (SWIGS)
60	NJ24	ELC	57.48527	−3.29783	UoS (SWIGS)
61	NO08	MAR	56.97714	−3.51987	UoS (SWIGS)
62	NN55	RAN	56.64078	−4.32966	UoS (SWIGS)
63	NO49	TAN	57.0344	−2.85374	UoS (SWIGS)
64	NO03	Birnam Wood (Birn)	56.52331	−3.49723	Junge et al.
65	NT86	Laveric Law	55.90761	−2.23836	Junge et al.
66	NN96	Pitlochry (Pilo)	56.72433	−3.66048	Junge et al.
67	NX87	Barfil	55.03643	−3.81730	Tauber et al.
68	NS50	Carsphairn Forest	55.31079	−4.21788	Tauber et al.
69	NX68	Holy Linn Waterfall	55.10922	−4.10558	Tauber et al.
70	NX78	Minnygryle Hill	55.18504	−4.03179	Tauber et al.

*Note.* BGS - British Geological Survey, UoE - University of Edinburgh, UoS - University of Southampton. Other legacy sites, see text for reference.

product from observatories is currently 1 min. In addition, to accurately derive MT impedances for periods of 10 s and below, it is necessary to use broadband rather than LMT equipment.

To visualize a larger number of sites on a spatial scale, it is useful to display MT impedances as phase tensor maps per period (Caldwell et al., 2004). Phase tensors are free from local galvanic distortion, but indicate changes in and the complexity of the electrical conductivity distribution at depth. Figure 5 shows the phase tensors at all 70 sites across Britain for six different periods (longer periods represent greater depths). Their shape and color indicate the wide variability of electrical conductivity at different depth levels in the UK, especially at shallower depths (32 s), while at larger depths there are more regional trends visible. For the shorter periods of up to 520 s, spatial variability between sites is large, indicating more complex geology.



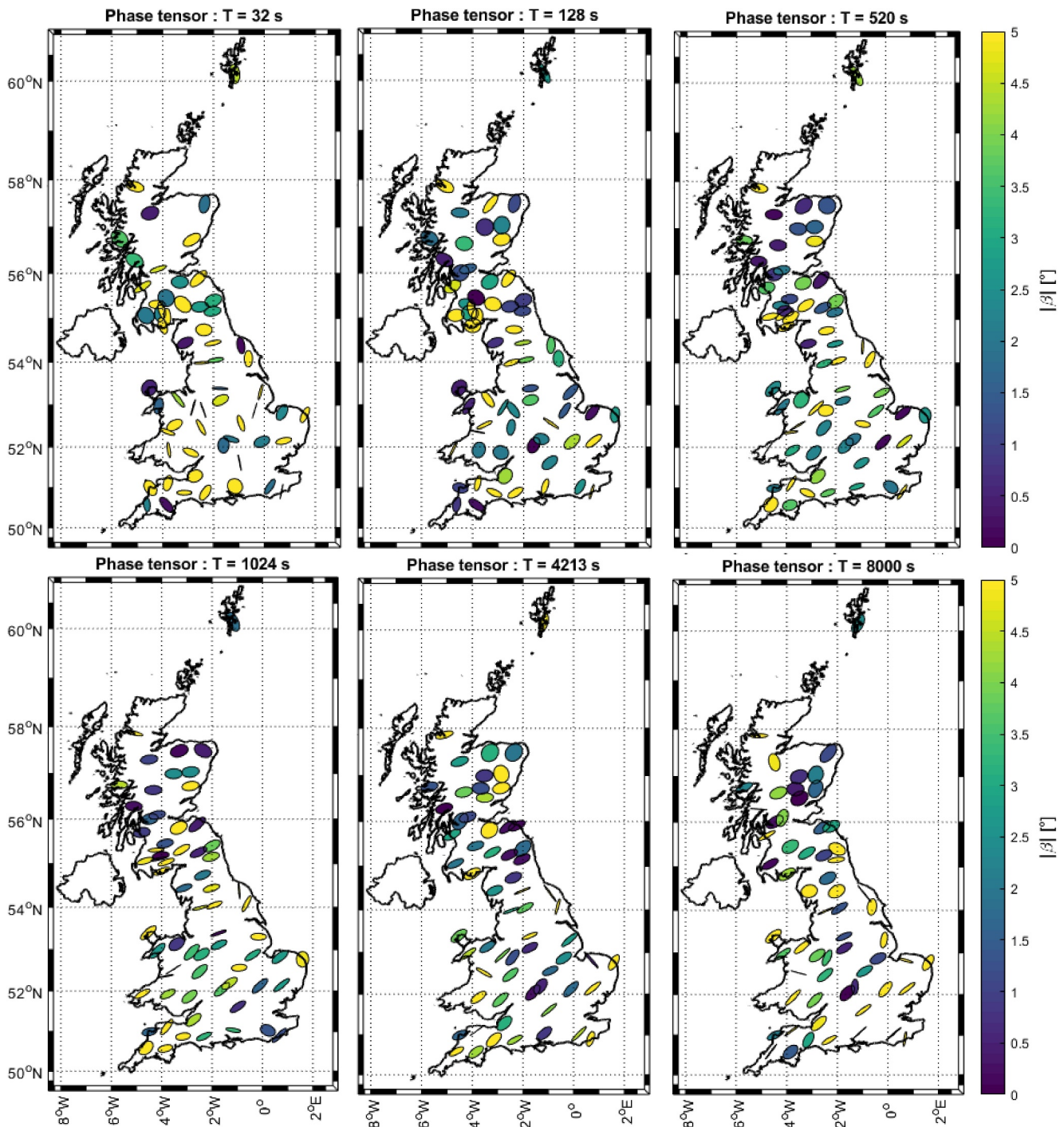


**Figure 5.** Magnetotelluric (MT) phase tensor estimates for SWIMMR Activities in Ground Effects MT sites and legacy data across Britain for six different periods. Upper panels: 32 s, 128 s, 520 s. Lower panels: 1024 s, 4213 s and 8000 s. The color fill is the skew angle  $\beta$  (after Caldwell et al. (2004)). Large spatial variability in the surface impedance is visible for all periods.

#### 2.4. Spatial Variability and Inter-Site Distance of MT Data Across Britain

With the presented MT data, the inter-site spacing across Britain is now mostly below 50 km, which corresponds to the commonly applied site spacing of large-scale MT arrays in, for example, the US and Australia (Duan, 2019; Kelbert et al., 2011). The distances to the nearest MT sites are visualized in Figure 6 (left panel). While a regular site spacing would be ideal, the presence of large urban areas and the rugged coastline of Britain create a natural

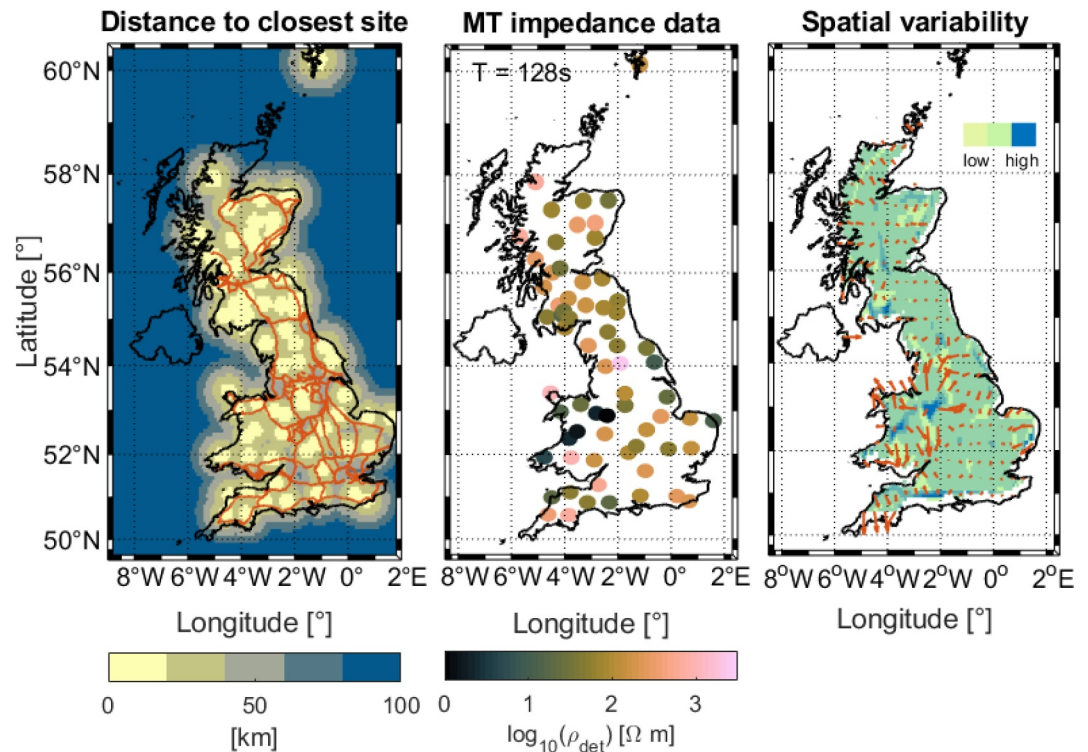


**Figure 6.** Left: Distance to closest magnetotelluric site in Britain. Orange lines indicate the location of 400 and 275 kV high voltage power lines. Middle: Apparent resistivity of the determinant of the impedance tensors at  $T = 128$  s. Right: Spatial variability of the apparent resistivity of the impedance tensor determinant. Darker colors indicate larger spatial variability. Arrows indicate the gradient with direction and amplitude of largest change.

limit. Additionally to the site spacing, the lateral variability of the MT data should be considered to evaluate if the resulting geoelectric field model is sufficiently resolved. In the presence of large spatial changes between sites due to strong geologic contrasts, a denser sampling might be necessary (Murphy et al., 2021). While a full 3D inversion model is in preparation, we seek to assess the spatial variability of the MT data set from an evaluation of the data itself.

The phase tensor representation of the MT impedance (as seen in Figure 5)—while capturing the lateral changes very well—does not contain information about the actual amplitude of the electric field. It is therefore more meaningful to look at a different representation of MT impedance data in a GIC-relevant period band to understand where inter-site spacing should be improved for evaluating geoelectric hazards across the country. The determinant of the impedance tensor ( $Z_{\text{det}}$ ), similar to the Berdichevsky average, has long been used in 2D MT data inversion practise and proven useful in strongly 3D areas before dense data coverage and 3D inversion algorithms became available (Pedersen & Engels, 2005). It represents an average of the full impedance tensor. Figure 6 (middle panel) depicts the apparent resistivity of the impedance determinant for 128 s. It is evident that there are very low apparent resistivities (below 3 Ωm) at sites in Wales and the north-west of England (the Cheshire sedimentary basin, around [53°N, 3°W]), bordered by very large apparent resistivities (above 1,000 Ωm) in the north of England, north-west of Wales and also present in north-west Scotland. Looking further at the largest lateral rate of change in ( $Z_{\text{det}}$ ) for the selected period (Figure 6, right panel), highlights that there are strong changes (represented by longer arrows) in the data in the north–west and the south–west of England as well as in the north of Scotland. This should be kept in mind for the analysis of the geoelectric field model below and will be addressed in future MT data collection campaigns.

### 3. Modeling the Geoelectric Field During Geomagnetic Storms

The new data set is now used to characterize the geoelectric field due to the ground response during geomagnetic storm times. We performed geoelectric field modeling for three geomagnetic storms of the past decades: the

March 1989 storm that caused wide-spread ground effects especially in Canada, the “Halloween” storm 29–31 October 2003 and the September 2017 storm.

We adapted the algorithm of Campanya et al. (2019) to calculate the electric field at all 70 sites during these major geomagnetic storms. The first step is to characterize the ground magnetic field variation across the entire country. This is done using the spherical elementary current systems (SECS) interpolation method (e.g., McLay & Beggan, 2010) based on measured magnetic data from several INTERMAGNET observatories and UK variometer sites. The availability of magnetic field data varies for historical storms and is higher in the last decade, when in addition to geomagnetic observatories, data from several variometer sites can be applied.

For the SECS interpolation of the March 1989 and October 2003 storm, one-min magnetic field data from the UK observatories (ESK, LER, HAD), and three further European INTERMAGNET observatories (CLF, VAL, WNG) were used. For September 2017, one-minute cadence data were available from the three UK observatories (ESK, LER, HAD), other European observatories around the North Sea and Ireland (CLF, DOU, VAL, WNG), the variometer sites from the Lancaster SAMNET, MagIE, Tromsø Geophysical Observatory and BGS School Magnetometer Network (ARM, BGS09, BGS10, BIR, CRK, DOB, HOV, SOL, KAR, SID) (Beggan & Marple, 2018). The magnetic field variations  $B_{SECS}$  across Britain were modeled on a  $10 \times 10$  km grid using the available observed data and then interpolated at the MT site locations. Similar to Campanya et al. (2019); Malone-Leigh et al. (2023), we then derived time-series of the geoelectric field for each geomagnetic event using:

$$E_{est}(t) = FFT^{-1} [Z(\omega) \cdot FFT(B_{SECS}(t))]$$

The horizontal components ( $B_x, B_y$ ) of the magnetic field at one-min cadence are interpolated at each MT location for the duration of two (for March 1989 and September 2017) or three days (October 2003), then Fourier-transformed to compute the equivalent values in frequency space. The Fourier coefficients were then multiplied by the MT impedance values and then inversely Fourier-transformed back into time domain. This produced the time-series of horizontal geoelectric field ( $E_x$  and  $E_y$ ) at each MT site during the storms in a frequency range dependent on the sampling rate of the magnetic field data and the period extent of the impedance tensor at each site (which varies due to data quality). We then performed a simple nearest-neighbor triangulation to interpolate the geoelectric field values across Britain onto a  $10 \times 10$  km grid. The interpolation onto a regular grid facilitates the modeling and nowcasting of GICs in ground-based infrastructure (Kelly et al., 2017).

To investigate the results, we first define the peak time of the geoelectric field during a geomagnetic storm as the minute with the highest value of the computed sum of the absolute geoelectric field values at all MT sites across the island of Britain. Figure 7 shows the time series of the sum of all modeled geoelectric field values for the three storms. For example, the peak of the March 1989 storm in Britain was at 21:45 UT on the 13th March (Figure 7, upper panel). Figure 8 shows the modeled geoelectric field components  $E_x$ ,  $E_y$  and the total horizontal field  $E_h = \sqrt{E_x^2 + E_y^2}$  as a snapshot at the peak times of each of the three storms. The direction and amplitude of the geoelectric field at each modeling point are indicated with an arrow. The overall largest geoelectric field values were modeled for the March 1989 storm. During the peak of the March 1989 storm, the largest field values are located in the north of England (exceeding 3 V/km), covering large areas in the narrow center of Britain as well as in the north of Scotland (see Figure 8, upper panels). This is due to a combination of a south-extended auroral zone (which causes the largest fluctuations in the magnetic field, e.g., Freeman et al. (2019)) and the local ground response as can be seen in the MT impedance data (see Figure 6 middle panel). The direction of the geoelectric field at the peak time points toward east and north-east in the center of Britain. For the peak of the October 2003 storm, the characteristics in the geoelectric field are similar to March 1989, with overall slightly lower modeled amplitudes (see Figure 8, middle panels). The values modeled in Scotland generally agree with previous modeling in Thomson et al. (2005). The direction of the peak geoelectric field is mostly eastwards in Scotland and at a south-east orientation in north England. In the third case for the September 2017 storm (see Figure 8, lower panels), the largest geoelectric field values are modeled for the north-west of Scotland, showing that the expansion of the auroral oval did not reach as far south as for the other two storms. The direction of the geoelectric field is mostly eastwards.

The geoelectric fields shown in Figure 8 only capture one temporal snapshot at the peak of each storm. Local maxima can occur at different times due to the moving of the auroral oval, but are relevant for assessing the impact

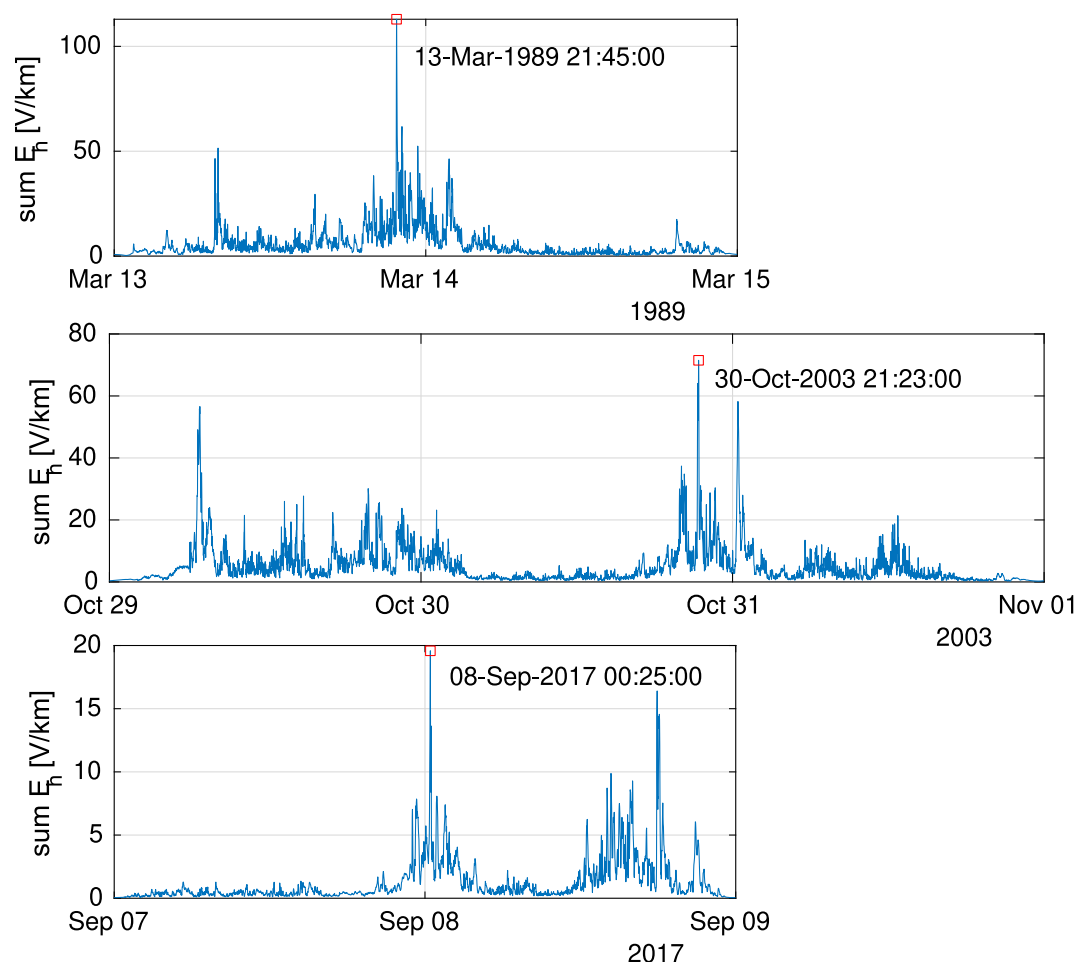


**Figure 7.** Sum of electric fields across all magnetotelluric sites during three geomagnetic storms (top: March 1989, middle: October 2003, bottom: September 2017). The peak times for each storm are indicated in the plot.

on grounded technology. We therefore also investigated the modeled time series for the overall maximum value at each MT site location. We estimated the maximum of the geoelectric field during the entire storm duration for the horizontal electric field ( $|E_h|$ ) at each individual site. These are plotted in Figure 9. The directions of the polarized electric field are indicated with arrows at each of the MT site locations. The top five sites for largest modeled geoelectric field for each of the three storms are listed within the figure. The maximum values can more clearly display the local response than the peak snapshot images in Figure 8 and assist in geoelectric risk assessments. We find that the largest modeled geoelectric field values actually exceed 8 V/km in central Britain during the March 1989 storm.

The direction of the electric field has direct implications for the overall effects on elongated grounded infrastructures like high-voltage power lines and gas pipelines, because GICs will become larger in conductors aligned with the direction of the geoelectric field. As can be seen in Figure 9, the direction of the largest fields tend to point E–W for sites in Scotland, whereas there is a NE–SW trend for sites in northern England and Wales. This behavior is similar in all three storm times, indicating that the direction of the geoelectric field mainly depends on the underlying conductivity, not on the variations in the source field. In Scotland, the longest HV power lines and main gas pipelines run north–south, but in England and Wales are connected east–west, with therefore a higher risk from large GICs in grounded systems. In the future, we will investigate this in more detail by reanalyzing GIC models (e.g., Kelly et al., 2017) using the new geoelectric field model.



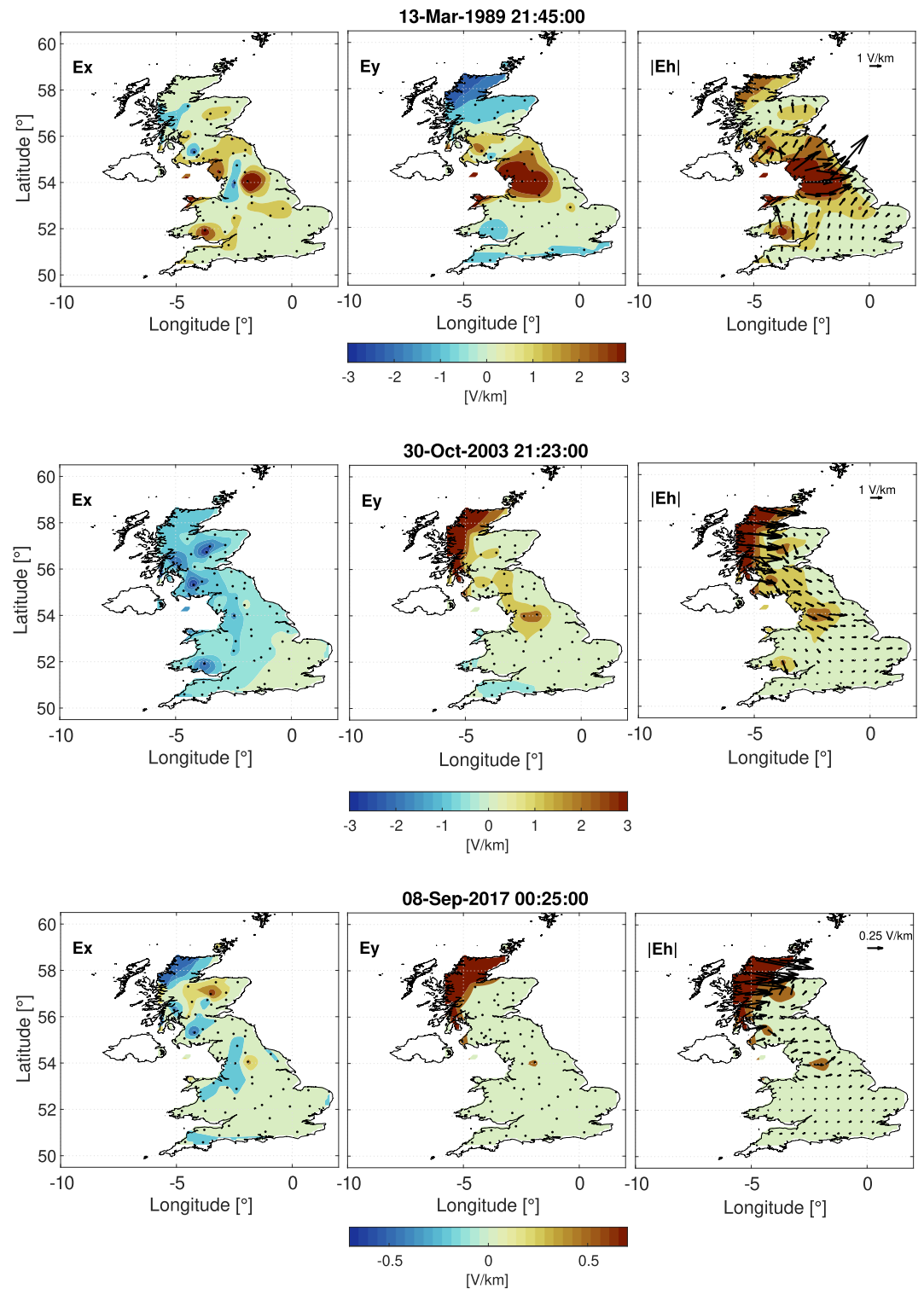


**Figure 8.** Snapshot of the geoelectric field model across Britain during the *peak* of the March 1989 (top), the October 2003 (middle), and the September 2017 (bottom) storm. Left panels:  $E_x$  (north–south component), middle panels:  $E_y$  (east–west component), right panels:  $|E_h|$  (absolute value of the horizontal electric field with arrows indicating the direction of the field).

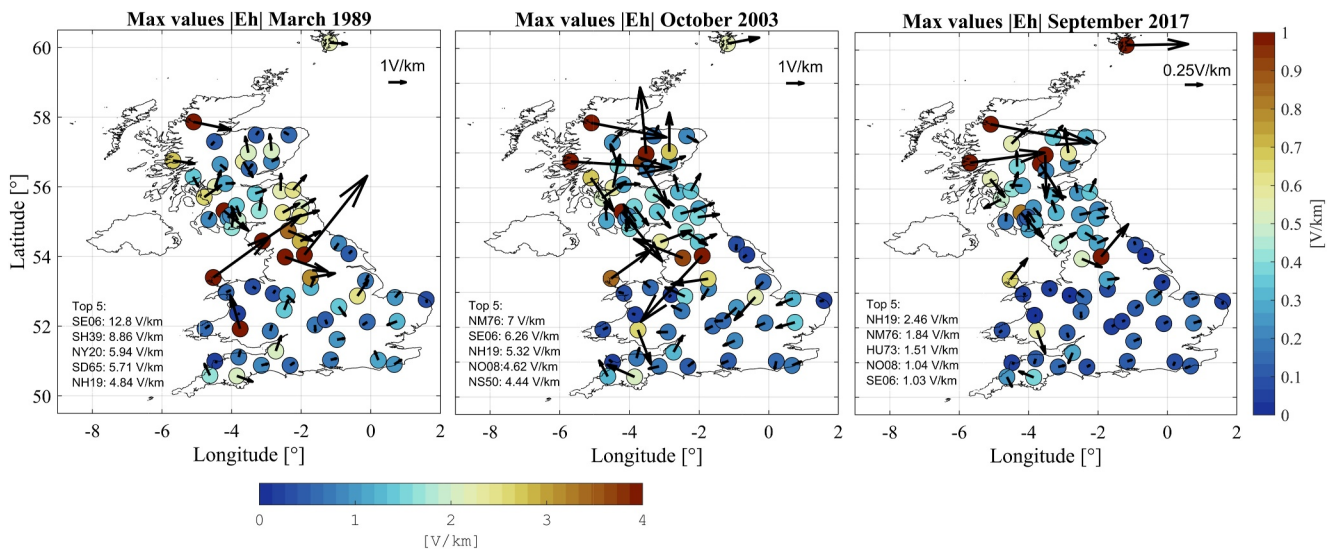


**Figure 9.** Comparison of *maximum* values of the horizontal electric field  $|E_h|$  at magnetotelluric site locations during three geomagnetic storms: March 1989, October 2003, and September 2017. The arrows additionally indicate the direction of the field. Note the different color scale and unit arrow length for September 2017. The inset tables list the five sites with the largest maximum electric field values modeled. For the location of these sites see Figure 1.

#### 4. Discussion

The new geoelectric field model presented refines the regional geoelectric hazard assessment in Britain, adding more detail to a long line of existing research and measurements (Beamish et al., 2002; McKay, 2003; Thomson et al., 2005; Beggan et al., 2013) and decreasing uncertainties in the lateral variations of the geoelectric field during storm times. With the new MT data collected at 53 sites and incorporating legacy data, the lateral variability of the geoelectric field is more accurately defined and highlights the influence of local geology.

As observed in the snapshot map analysis, there are distinct differences in the spatial distribution of the highest geoelectric field amplitudes. For the 2017 storm, there is a clear occurrence of the highest amplitudes at higher latitudes, showing maximum values for the Scottish Highlands ( $>1.5$  V/km). However, for the 1989 storm, the largest geoelectric field values were reached in northern England (exceeding 8 V/km). This was caused by the combination of a the strong south expansion of the auroral oval during this major geomagnetic event and the local geoelectric response from subsurface geology.

In the 2003 storm simulation, the largest peak values were reached in Scotland with almost equally high amplitudes in northern England ( $\sim 6$ – $7$  V/km).

Assessing the local geoelectric response based on surface geology is challenging. The electrical conductivity of the bedrock in the UK was characterized in detail by Beamish (2013). For the assessment of space weather impacts however, knowledge of the deeper lithosphere is needed corresponding to the larger penetration depth of the longer period signals generated by the interaction of the solar wind with the Earth's magnetic field. The areas with the highest amplitudes of the geoelectric field are the north of Scotland, the north of England and the northwestern part of Wales. In the north of Scotland and Wales, bedrock electrical conductivity is generally low (see Figure 1, 0.3–2 mS/m after Beamish (2013)), which matches the observed higher amplitudes of geoelectric fields in our model. In contrast, the sites in the north of England showing the strongest geoelectric fields (SE06 and SD65) in the March 1989 and October 2003 storms are located in areas with only medium bedrock electrical conductivity (8–16 mS/m). This would indicate that at greater depth there must be more resistive rocks overlain by a more conductive layer that dictate the amplitude of geoelectric field in the space weather relevant period range.

Murphy et al. (2021) suggested that, depending on local geology, it would be beneficial to include higher frequency MT data (broadband: 100–0.1 Hz) to better represent the local geoelectric field during storms. In the absence of large-scale broadband MT data in the UK, and few locations where magnetic field data are sampled at higher frequencies (Beggan & Musur, 2018), we acknowledge the frequency limitations of the geoelectric field

model, most likely to result in a slight underestimation of the amplitude as observed and discussed by Beggan et al. (2021). Nevertheless, the achieved spatial coverage can for the first time give reliable estimates of the peak geoelectric field values related to geomagnetic storms observed in the past decades. These new results form the basis for a more in-depth analysis of extreme values for a geoelectric hazard assessment in the UK, highlighting regions where vulnerability is greater than previously expected.

In the future, it is desirable to decrease MT site spacing with more measurements, especially in areas of strong lateral variability like north-west England and areas with GIC sensitive assets like the west and east coast railway lines. Coverage in the south-east of England should also be improved to decrease uncertainties in the geoelectric field model. We will also use the new geoelectric field model to create geoelectric hazard maps for the UK using extreme value analysis, to look at the hazard posed to railway signaling and incorporate the new data into now- and forecasting of space weather ground effects.

Furthermore, the data will be used to derive a new three-dimensional electrical conductivity model of the lithosphere below Britain, imaging the many tectonic boundaries known from geological, airborne and seismic surveys. This new 3D lithospheric model will help to further improve the geoelectric field and GIC modeling by deriving impedance tensors at any location in the UK, which will produce a smoother geoelectric field model by replacing the mathematical interpolation between MT sites with the more physically representative results from inverse modeling (Alves Ribeiro et al., 2023; Torta et al., 2023).

## 5. Conclusions

We present new LMT data from 53 sites in Britain collected between 2021 and 2024 under the SWIMMR program. The general data quality benefitted from increased geomagnetic activity during the recording and it was possible to derive stable MT impedance estimates for periods ranging from 16 to 20,000 s. Additionally, we examined available legacy MT data in Britain to improve spatial sampling. In total, data from 70 MT sites were used in the new geoelectric field model. We examined the spatial variability in the impedance data and identified areas in west England and Wales with large local variations that would greatly benefit from additional MT data collection to increase resolution in the geoelectric field model and decrease uncertainties in the onward modeling of space weather effects on grounded systems.

Using the MT impedances we computed geoelectric field time series at all MT sites for three of the largest storms in the digital era, March 1989, October 2003, and September 2017, using SECS-interpolated geomagnetic field data from UK observatories and variometer sites, sampled at one minute. We observed that there are large spatial variations in geoelectric field amplitudes due to the local ground response that vary with the intensity of the storm and the position and southward extent of the auroral oval zone. Investigating the peak times of each storm and maximum field values revealed that several previously unknown regions in central Britain can experience large field values, potentially up to 12 V/km in northern England.

The new data set is openly available and will be used to establish the space weather hazard in terms of GICs in grounded infrastructure in Great Britain as well geological imaging and modeling of the subsurface tectonic structure.

## Acknowledgments

We thank BGS staff for their assistance with MT field work: Adam Collins, Helen Smith, Guanren Wang, Sarah Watson, Dave Morgan and Eleanor Maume. We thank the many landowners for allowing access to their land for the temporary deployment of the MT systems. This project was funded under the NERC SWIMMR Activities in Ground Effects (SAGE), Grant number NE/V002694/1 from June 2020 to March 2024. Nine LMT sites in Scotland were collected jointly by University of Edinburgh and BGS with funding from the Scottish Alliance for Geoscience, Environment and Society (SAGES) and a Grant from the Royal Astronomical Society. This paper is published with the permission of the Executive Director of the British Geological Survey (UKRI).

## Data Availability Statement

Magnetotelluric measurements collected during the SAGE project are available on the NERC Geoscience Data Center (NGDC) <https://www.bgs.ac.uk/geological-data/national-geoscience-data-center/>. The *aa* index is available from the World Data Centre for Geomagnetism in Edinburgh <http://www.wdc.bgs.ac.uk/data>. Magnetic field data from the UK and European observatories are available via the INTERMAGNET website <https://www.intermagnet.org>. Variometer data are available via the Lancaster Aurorawatch website <https://aurorawatch.lancs.ac.uk/> and MagIE data are available at <https://data.magie.ie/>.

## References

- Alves Ribeiro, J., Pinheiro, F. J. G., Pais, M. A., Santos, R., Cardoso, J., Baltazar-Soares, P., & Monteiro Santos, F. A. (2023). Toward more accurate GIC estimations in the Portuguese power network. *Space Weather*, 21(6), e2022SW003397. <https://doi.org/10.1029/2022SW003397>
- Ayala, C., Beamud, E., Huebert, J., Jones, S. A., Kumar, A., Miller, S. R., et al. (2022). Geomagnetism, paleomagnetism and electromagnetism perspectives on integrated, coordinated, open, networked (ICON) science. *Earth and Space Science*, 9(6), e2021EA002141. <https://doi.org/10.1029/2021EA002141>

- Beamish, D. (2012). *The 1:625k near-surface bedrock electrical conductivity map of the UK*. (Tech. Rep. No. OR/12/037). British Geological Survey. Retrieved from <http://nora.nerc.ac.uk/20833/23pp>
- Beamish, D. (2013). The bedrock electrical conductivity map of the UK. *Journal of Applied Geophysics*, 96, 87–97. <https://doi.org/10.1016/j.jappgeo.2013.06.001>
- Beamish, D., Clark, T., Clarke, E., & Thomson, A. (2002). Geomagnetically induced currents in the UK: Geomagnetic variations and surface electric fields. *Journal of Atmospheric and Solar-Terrestrial Physics*, 64(16), 1779–1792. [https://doi.org/10.1016/S1364-6826\(02\)00127-X](https://doi.org/10.1016/S1364-6826(02)00127-X)
- Beggan, C. D. (2015). Sensitivity of geomagnetically induced currents to varying auroral electrojet and conductivity models. *Earth Planets and Space*, 67(1), 1–12. <https://doi.org/10.1186/s40623-014-0168-9>
- Beggan, C. D., Beamish, D., Richards, A., Kelly, G. S., & Thomson, A. W. P. (2013). Prediction of extreme geomagnetically induced currents in the UK high-voltage network. *Space Weather*, 11(7), 407–419. <https://doi.org/10.1002/swe.20065>
- Beggan, C. D., Eastwood, J. P., Eggington, J. W. B., Forsyth, C., Freeman, M. P., Henley, E., et al. (2025). Implementing an operational cloud-based now- and forecasting system for space weather ground effects in the UK. *Space Weather*, 23(5), e2025SW004364. <https://doi.org/10.1029/2025SW004364>
- Beggan, C. D., & Marple, S. R. (2018). Building a Raspberry Pi school magnetometer network in the UK. *Geoscience Communication*, 1(1), 25–34. <https://doi.org/10.5194/gc-1-25-2018>
- Beggan, C. D., & Musur, M. (2018). Observation of ionospheric Alfvén resonances at 1–30 Hz and their superposition with the schumann resonances. *Journal of Geophysical Research: Space Physics*, 123(5), 4202–4214. <https://doi.org/10.1029/2018JA025264>
- Beggan, C. D., Richardson, G. S., Baillie, O., Hübert, J., & Thomson, A. W. P. (2021). Geoelectric field measurement, modelling and validation during geomagnetic storms in the UK. *Journal of Space Weather and Space Climate*, 11, 37. <https://doi.org/10.1051/swsc/2021022>
- Bolduc, L. (2002). GIC observations and studies in the Hydro-Québec power system. *Journal of Atmospheric and Solar-Terrestrial Physics*, 64(16), 1793–1802. [https://doi.org/10.1016/S1364-6826\(02\)00128-1](https://doi.org/10.1016/S1364-6826(02)00128-1)
- Boteler, D. H. (2006). The super storms of August/September 1859 and their effects on the telegraph system. *Advances in Space Research*, 38(2), 159–172. <https://doi.org/10.1016/j.asr.2006.01.013>
- Boteler, D. H. (2019). A 21st century view of the March 1989 magnetic storm. *Space Weather*, 17(10), 1–15. <https://doi.org/10.1029/2019SW002278>
- Cagniard, L. (1953). Basic theory of the magnetotelluric method of geophysical prospecting. *Geophysics*, 18(3), 605–635. <https://doi.org/10.1190/1.1437915>
- Caldwell, T. G., Bibby, H. M., & Brown, C. (2004). The magnetotelluric phase tensor. *Geophysical Journal International*, 158(2), 457–469. <https://doi.org/10.1111/j.1365-246X.2004.02281.x>
- Campanya, J., Gallagher, P. T., Blake, S. P., Gibbs, M., Jackson, D., Beggan, C., et al. (2019). Modeling geoelectric fields in Ireland and the UK for space weather applications. *Space Weather*, 17(2), 216–237. <https://doi.org/10.1029/2018SW001999>
- Chave, A. D., & Jones, A. G. (2012). *The magnetotelluric method: Theory and practice*. Cambridge University Press.
- Cordell, D., Unsworth, M. J., Lee, B., Hanneson, C., Milling, D. K., & Mann, I. R. (2021). Estimating the geoelectric field and electric power transmission line voltage during a geomagnetic storm in Alberta, Canada using measured magnetotelluric impedance data: The influence of three-dimensional electrical structures in the lithosphere. *Space Weather*, 19(10), e2021SW002803. <https://doi.org/10.1029/2021sw002803>
- Dong, S. W., Li, T. D., Lü, Q. T., Gao, R., Yang, J. S., Chen, X. H., et al. (2013). Progress in deep lithospheric exploration of the continental China: A review of the sinoprobe. *Tectonophysics*, 606, 1–13. <https://doi.org/10.1016/j.tecto.2013.05.038>
- Duan, J. (2019). *Resistivity model derived from magnetotellurics: Auslamp-tisa project*. Geoscience Australia. <https://doi.org/10.26186/5d5e24d062977>
- Egbert, G. (1997). Robust multiple-station magnetotelluric data processing. *Geophysical Journal International*, 130(2), 475–496. <https://doi.org/10.1111/j.1365-246X.1997.tb05663.x>
- Freeman, M. P., Forsyth, C., & Rae, I. J. (2019). The influence of substorms on extreme rates of change of the surface horizontal magnetic field in the United Kingdom. *Space Weather*, 17(6), 827–844. <https://doi.org/10.1029/2018SW002148>
- Gamble, T. D., Goubau, W. M., & Clarke, J. (1979). Magnetotellurics with a remote magnetic reference. *Geophysics*, 44(1), 53–68. <https://doi.org/10.1190/1.1440923>
- Hübert, J., Beggan, C., Richardson, G. S., Gomez-Perez, N., Collins, A., & Thomson, A. W. P. (2024). Validating a UK geomagnetically induced current model using differential magnetometer measurements. *Space Weather*, 22(2), e2023SW003769. <https://doi.org/10.1029/2023SW003769>
- Hübert, J., Beggan, C. D., Richardson, G. S., Martyn, T., & Thomson, A. W. P. (2020). Differential magnetometer measurements of geomagnetically induced currents in a complex high voltage network. *Space Weather*, 18(4), e2019SW002421. <https://doi.org/10.1029/2019SW002421>
- Hübert, J., Eaton, E., Beggan, C., Collins, A., & Wang, G. (2025). Long-period magnetotelluric data collected at 44 sites in Scotland, England and Wales [Dataset]. *NERC EDS National Geoscience Data Centre*. <https://doi.org/10.5285/14274b67-86a5-4d9d-b3f4-20c6d20228d7>
- Jankowski, J., & Sucksdorff, C. (1996). IAGA guide for magnetic measurements and observatory practice. *International Association of Geomagnetism and Aeronomy*.
- Junge, A. (1995). Magnetotellurics in the long period range, final report. *Technical report, EEC Human Capital and Mobility contract No. ERBCHBICT 93*, 142–151. 0610.
- Karato, S.-i., & Wang, D. (2013). 01). Electrical conductivity of minerals and rocks. *Physics and Chemistry of the Deep Earth*, 1–144.
- Kelbert, A., Balch, C. C., Pulkkinen, A., Egbert, G. D., Love, J. J., Rigler, E. J., & Fujii, I. (2017). Methodology for time-domain estimation of storm time geoelectric fields using the 3-D magnetotelluric response tensors. *Space Weather*, 15(7), 874–894. <https://doi.org/10.1002/2017SW001594>
- Kelbert, A., Egbert, G., & Schultz, A. (2011). Iris dmc data services products: Emtf, the magnetotelluric transfer functions. *IRIS DMC*. <https://doi.org/10.1190/geo2018-0679.1>
- Kelly, G. S., Viljanen, A., Beggan, C., & Thomson, A. W. P. (2017). Understanding GIC in the UK and French high-voltage transmission systems during severe magnetic storms. *Space Weather*, 15(1), 99–114. <https://doi.org/10.1002/2016SW001469>
- Kruglyakov, M., Kuvshinov, A., & Marshalko, E. (2022). Real-Time 3-D modeling of the ground electric field due to space weather events. A concept and its validation. *Space Weather*, 20(4), e2021SW002906. <https://doi.org/10.1029/2021SW002906>
- Livelybrooks, D., Banks, R., Parr, R., & Hutton, V. (1993). Inversion of electromagnetic induction data for the iapetus suture zone in the UK. *Physics of the Earth and Planetary Interiors*, 81(1), 67–84. [https://doi.org/10.1016/0031-9201\(93\)90124-R](https://doi.org/10.1016/0031-9201(93)90124-R)
- Love, J. J., Lucas, G. M., Kelbert, A., & Bedrosian, P. A. (2018). Geoelectric hazard maps for the mid-atlantic United States: 100 year extreme values and the 1989 magnetic storm. *Geophysical Research Letters*, 45(1), 5–14. <https://doi.org/10.1002/2017GL076042>



- Malone-Leigh, J., Campaña, J., Gallagher, P. T., Neukirch, M., Hogg, C., & Hodgson, J. (2023). Nowcasting geoelectric fields in Ireland using magnetotelluric transfer functions. *Journal of Space Weather and Space Climate*, 13, 6. <https://doi.org/10.1051/swsc/2023004>
- Marshallko, E., Kruglyakov, M., Kuvshinov, A., Juusola, L., Kwagala, N. K., Sokolova, E., & Pilipenko, V. (2021). Comparing three approaches to the inducing source setting for the ground electromagnetic field modeling due to space weather events. *Space Weather*, 19(2), e2020SW002657. <https://doi.org/10.1029/2020SW002657>
- McKay, A. (2003). *Geoelectric fields and Geomagnetically Induced Currents in the United Kingdom*. Doctoral dissertation, University of Edinburgh. Retrieved from <https://era.ed.ac.uk/handle/1842/639>
- McLay, S. A., & Beggan, C. (2010). Interpolation of externally-caused magnetic fields over large sparse arrays using spherical elementary current systems. *Annales Geophysicae*, 28(9), 1795–1805. <https://doi.org/10.5194/angeo-28-1795-2010>
- Montiel-Álvarez, A., Collins, A., Wang, G., Hübert, J., & Beggan, C. (2025). Long-period magnetotelluric time series at 9 sites in Scotland, UK [Dataset]. *NERC EDS National Geoscience Data Centre*. <https://doi.org/10.5285/1d5f975c-4a12-4c9d-8808-315afb33fe10>
- Murphy, B. S., Lucas, G. M., Love, J. J., Kelbert, A., Bedrosian, P. A., & Rigler, E. J. (2021). Magnetotelluric sampling and geoelectric hazard estimation: Are national-scale surveys sufficient? *Space Weather*, 19(7), e2020SW002693. <https://doi.org/10.1029/2020SW002693>
- Oughton, E. J., Haggood, M., Richardson, G. S., Beggan, C. D., Thomson, A. W. P., Gibbs, M., et al. (2018). A risk assessment framework for the socioeconomic impacts of electricity transmission infrastructure failure due to space weather: An application to the United Kingdom. *Risk Analysis*, 38(12), 1–22. <https://doi.org/10.1111/risa.13229>
- Pedersen, L. B., & Engels, M. (2005). Routine 2D inversion of magnetotelluric data using the determinant of the impedance tensor. *Geophysics*, 70(2), G33–G41. <https://doi.org/10.1190/1.1897032>
- Pratscher, K. M., Ingham, M., Mac Manus, D. H., Kruglyakov, M., Heise, W., Rodger, C. J., et al. (2024). Modeling GIC in the southern south Island of aotearoa New Zealand using magnetotelluric data. *Space Weather*, 22(7), e2024SW003907. <https://doi.org/10.1029/2024SW003907>
- Pulkkinen, A., Bernabeu, E., Eichner, J., Beggan, C., & Thomson, A. (2012). Generation of 100-year geomagnetically induced current scenarios. *Space Weather*, 10(4), S04003. <https://doi.org/10.1029/2011SW000750>
- Rogers, N. C., Wild, J. A., Eastoe, E. F., Gjerloev, J. W., & Thomson, A. W. P. (2020). A global climatological model of extreme geomagnetic field fluctuations. *Journal of Space Weather and Space Climate*, 10, 5. <https://doi.org/10.1051/swsc/2020008>
- Rosenqvist, L., & Hall, J. O. (2019). Regional 3-D modeling and verification of geomagnetically induced currents in Sweden. *Space Weather*, 17(1), 27–36. <https://doi.org/10.1029/2018SW002084>
- Schultz, A. (2009). EMscope: A continental scale magnetotelluric observatory and data discovery resource. *Data Science Journal*, 8, IGY6–IGY20. [https://doi.org/10.2481/dsj.ss\\_igy-009](https://doi.org/10.2481/dsj.ss_igy-009)
- Simpson, F., & Bahr, K. (2021). Nowcasting and validating Earth's electric field response to extreme space weather events using magnetotelluric data: Application to the September 2017 geomagnetic storm and comparison to observed and modeled fields in Scotland. *Space Weather*, 19(1), e2019SW002432. <https://doi.org/10.1029/2019SW002432>
- Smirnov, M. Y. (2003). Magnetotelluric data processing with a robust statistical procedure having a high breakdown point. *Geophysical Journal International*, 152(1), 1–7. <https://doi.org/10.1046/j.1365-246X.2003.01733.x>
- Tauber, S., Banks, R., Ritter, O., & Weckmann, U. (2003). A high-resolution magnetotelluric survey of the iapetus suture zone in southwest Scotland. *Geophysical Journal International*, 153(3), 548–568. <https://doi.org/10.1046/j.1365-246X.2003.01912.x>
- Thomson, A. W. P., Dawson, E. B., & Reay, S. J. (2011). Quantifying extreme behavior in geomagnetic activity. *Space Weather*, 9(10), S10001. <https://doi.org/10.1029/2011SW000696>
- Thomson, A. W. P., McKay, A. J., Clarke, E., & Reay, S. J. (2005). Surface electric fields and Geomagnetically induced currents in the Scottish power grid during the 30 October 2003 geomagnetic storm. *Space Weather*, 3(11), S11002. <https://doi.org/10.1029/2005SW000156>
- Torta, J. M., Marsal, S., Piña-Varas, P., Hafizi, R., Martí, A., Campaña, J., et al. (2023). Expected geomagnetically induced currents in the Spanish Islands power transmission grids. *Space Weather*, 21(7), e2023SW003426. <https://doi.org/10.1029/2023SW003426>
- Turnbull, K. (2010). Modelling GIC in the UK. *Astronomy and Geophysics*, 51(5), 25–26. <https://doi.org/10.1111/j.1468-4004.2010.51525.x>
- Vasseur, G., & Weidelt, P. (1977). Bimodal electromagnetic induction in non-uniform thin sheets with an application to the northern pyrenean induction anomaly. *Geophysical Journal International*, 51(3), 669–690. <https://doi.org/10.1111/j.1365-246X.1977.tb04213.x>